

ELECTRONIC SUPPLEMENTARY INFORMATION

Phonons Spreading from Laser-Heated Gold Nanoparticle Array Accelerate Diffusion of Excitons in Underlying Polythiophene Thin Film

David Rais, Miroslav Menšík, Bartosz Paruzel, Dharmalingam Kurunthu and Jiří Pflieger*

Institute of Macromolecular Chemistry, AS CR, v.v.i., Heyrovského nám. 2, 162 06 Prague,
Czech Republic

Experimental

Transient absorption spectroscopy

A *pump-probe* transient absorption (TA) spectrometer HELIOS (Ultrafast Systems LLC) was used for the time resolved absorption spectroscopy measurements. The sample excitation (*pump*) was done by laser pulses with a central wavelength 550 nm and 12 nm FWHM, emitted from a two-stage optical parametric amplifier (Light Conversion Ltd., TOPAS-C). They were directed through a Berek's compensator (Newport, model 5540), which was adjusted to act as a half-wave plate to rotate the linear polarization of the *pump* pulses to the magic angle with respect to the orientation of the polarization of the *probe* pulses in the sample. The pulses were focused on the sample using a plano-convex spherical lens. The cross-section of the *pump* pulse fluence in the focal plane could be fitted with Gaussian beam profile with radius $r_{\text{pump}} = 270 \mu\text{m}$ (defined as the radius where the intensity of the pump beam equals to $1/e^2$ of the maximum intensity). Every second *pump* pulse was selected for the sample excitation using a synchronized mechanical chopper (excitation repetition rate 500 Hz), pulse energy was adjusted by a reflective neutral-density filter to the required energy, typically $1 \mu\text{J}/\text{pulse}$.

The sample was mounted to a XY translation stage, which allowed continuous scanning of the focal point of the laser across the sample area of ca. $5 \times 5 \text{ mm}$. The speed of 1 mm/s was enough to avoid experimental artifacts due to long-living states accumulation.

Probe laser pulses were derived from the output of a regenerative amplifier (Coherent Inc., LEGEND Elite USP), passed through a translation stage delay line (maximum delay 6 ns), and focused with a spherical mirror onto a sapphire crystal or a proprietary NIR-WLC generation crystal obtained from Ultrafast Systems to generate white-light continuum (WLC) in the spectral range of 400–750 nm (vis-WLC) or in the near-infrared (NIR) region, respectively. The vis-WLC beam was then split into two branches (sample and reference).

The beam in the sample branch was focused to fully overlap with the *pump*-pulse excited area of the sample. The cross-section of the *probe* pulse fluence in the focal plane (sample area) could be fitted with Gaussian beam profile with the radius $r_{\text{probe}} = 70 \mu\text{m}$ (defined as the radius where the intensity of the probe beam is $1/e^2$ times the maximum intensity). After passing the sample the probe pulses were filtered with a polarizer to remove the scattered light from the pump and passed a special filter (the reference probe pulses as well) to remove residual of the fundamental radiation (800 nm, from regenerative amplifier) and collected to the optical fiber input ports of two identical CCD-based spectrometers.

For the measurements in the NIR range (850–1200 nm) we had only one detector array available, thus we could use only measurement of un-pumped sample light transmission as a reference. Due to lack of dedicated reference detector the NIR-WLC measurement showed a lower signal-to-noise ratio, compared to the measurement with Vis-WLC. The high noise level also called for FFT-based noise filtering treatment, as will be described below.

NIR-WLC TA data refinement:

The original TA data acquired with NIR-WLC probe contained periodic experimental artifact noise, probably caused by periodic fluctuations of the laser system. It could be observed as horizontal strips (simultaneous fluctuations of the whole probe spectrum). The NIR-WLC TA data are more prone to this kind of instability than the vis-WLC, due to single-channel spectrometer configuration.

In order to remove the periodic instrumental artifact, FFT filtering was performed to remove the periodic fluctuation in the probe. In Figure S1, one can clearly observe the reduction of noise by filtering, especially at longer wavelengths.

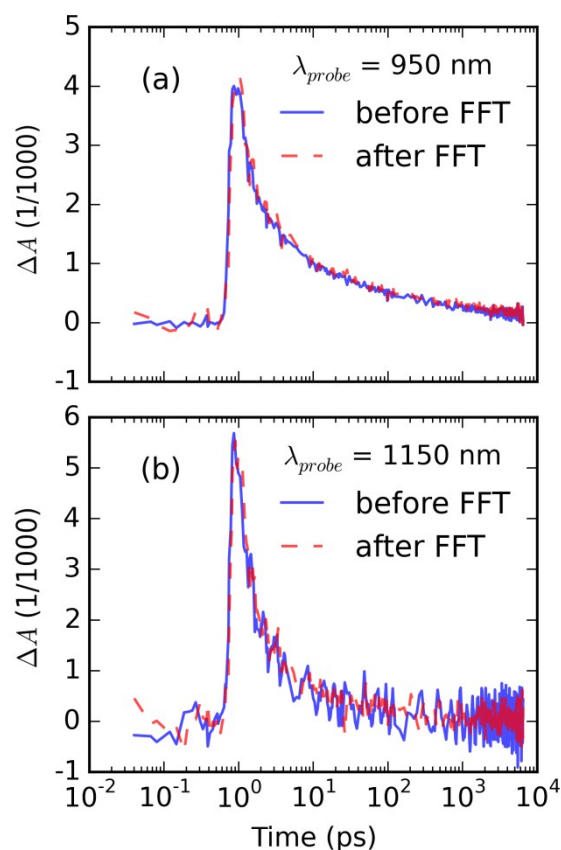


Figure S1. Comparison of selected time traces before and after FFT filtering of the data obtained with AuNP@P3HT sample. Probe wavelengths are indicated in the respective legends.

Results

TA signals evolution in AuNP@PS

The TA spectra of AuNP@PS sample deposited on glass substrate are shown in Figure S2. They were recorded following photoexcitation with laser pulses of 550 nm central wavelength, 0.5 $\mu\text{J}/\text{pulse}$.

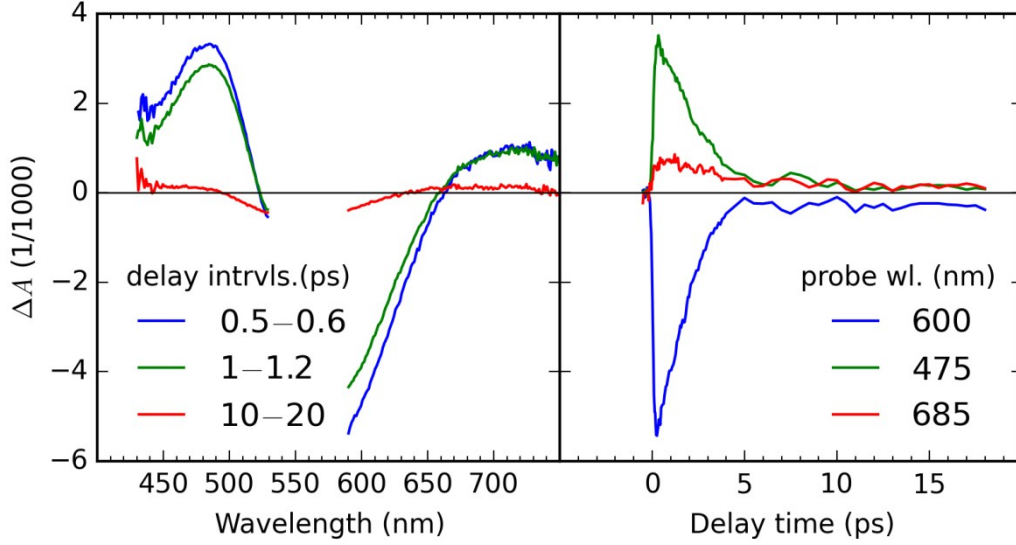


Figure S2. (a) The representative TA spectra of AuNP@PS system for pump power $0.5 \mu\text{J}$ averaged over selected intervals of the delay time (as indicated in the legend). The probe wavelength region 530–580 nm was removed due to the high content of scattered pump light. (b) The representative kinetic traces at selected probe wavelengths (as indicated in the legend).

Target model analysis of the vis-WLC transient absorption data

A *global* and *target analysis* of the TA data were performed to gain insight into the transformations of the excited state. In an attempt to rationalize the observed spectro-temporal TA data $\Delta A(t, \lambda)$ a *target analysis* method is used.¹ It allows to obtain so-called *Species-Associated Differential Spectra* (SADS)^{1,2} $\varepsilon_i(\lambda)$ and evolutions of their populations $c_i(t)$, through separation of the obtained TA data into the set of components i :

$$\Delta A(t, \lambda) = \sum_i c_i(t) \varepsilon_i(\lambda) \quad (1)$$

where t is the delay time between the pump and probe pulses, and λ is the probe wavelength. The fitting of the kinetic models was performed with Glotaran and TIMP software.^{3,4}

Analysis of TA signals of AuNP@PS

Using *global analysis* approach with a sequential, unbranched compartmental model,^{1,2,5} we could identify 3 exponential signal decay times τ_i : 0.57, 1.2 and 9.9 ps for $i \in \{1, 2, 3\}$, respectively (see the Figures S3a,d), that fell within the time-resolution limits of our equipment. The three processes probably reflect the various stages of relaxation of the photo-excited electron gas within the AuNP array; as discussed in details in the main text. The most significant component was that one with the lifetime 1.2 ps. This component was chosen for inclusion in model of the AuNP@P3HT composite thin film as representing the evolution due to the AuNP array plasmon absorption.

Kinetic model for the AuNP@P3HT composites

We constructed a model for the composite AuNP@P3HT, in which the excitation of AuNP array evolves independently on the excited states evolution of the underlying P3HT-film. This approach is motivated by the desire to observe the influence of the AuNPs array on the excitation evolution in the P3HT film. For this it should be helpful to compare the evolutions of the excited states in the polymer film with and without AuNPs array. The relatively short-lived excitation of electron gas in the metal particle array is represented with a single lifetime, whereas the evolution in P3HT film is represented by sequential decay of the excited states. The model system of kinetic equations for populations (fractional) $c_i(t)$ of the excited states the can be written as follows:

$$\begin{aligned}
\frac{d}{dt}c_1 &= \varphi_{\text{ex}}j_p(t) - \frac{c_1}{\tau_1} \\
\frac{d}{dt}c_2 &= \frac{c_1}{\tau_1} - \frac{c_2}{\tau_2} \\
\frac{d}{dt}c_3 &= \frac{c_2}{\tau_2} - \frac{c_3}{\tau_3} \\
\frac{d}{dt}c_4 &= \frac{c_3}{\tau_3} - \frac{c_4}{\tau_4} \\
\frac{d}{dt}c_5 &= \frac{c_4}{\tau_4} - \frac{c_5}{\tau_5} \\
\frac{d}{dt}c_6 &= (1 - \varphi_{\text{ex}})j_p(t) - \frac{c_6}{\tau_6}
\end{aligned} \tag{2}$$

Here, t denotes the time. The term $j_p(t) = \exp(-t^2/2\tau_p^2)$ represents the approximation of the temporal instrument response function (IRF), mainly governed by the time envelope of the pump pulse. The (Gaussian) time constant τ_p , as well as the lifetimes $\tau_i, i \in \{1..6\}$ in our model were taken as free parameters and they were optimized using TIMP software algorithms. The value of the branching weight factor was chosen $\varphi_{\text{ex}} = 0.5$ for the AuNP@P3HT composite thin film. In the case of neat P3HT film, the value $\varphi_{\text{ex}}=1$, effectively deactivated the AuNPs array excitation branch, i.e. $c_6 \equiv 0$.

The resulting SADS together with the selected representative fits of kinetic traces for the neat P3HT and AuNP@P3HT systems are presented in Figures S3b,e and S3c,f, respectively. The Table S1 summarizes the obtained model lifetimes.

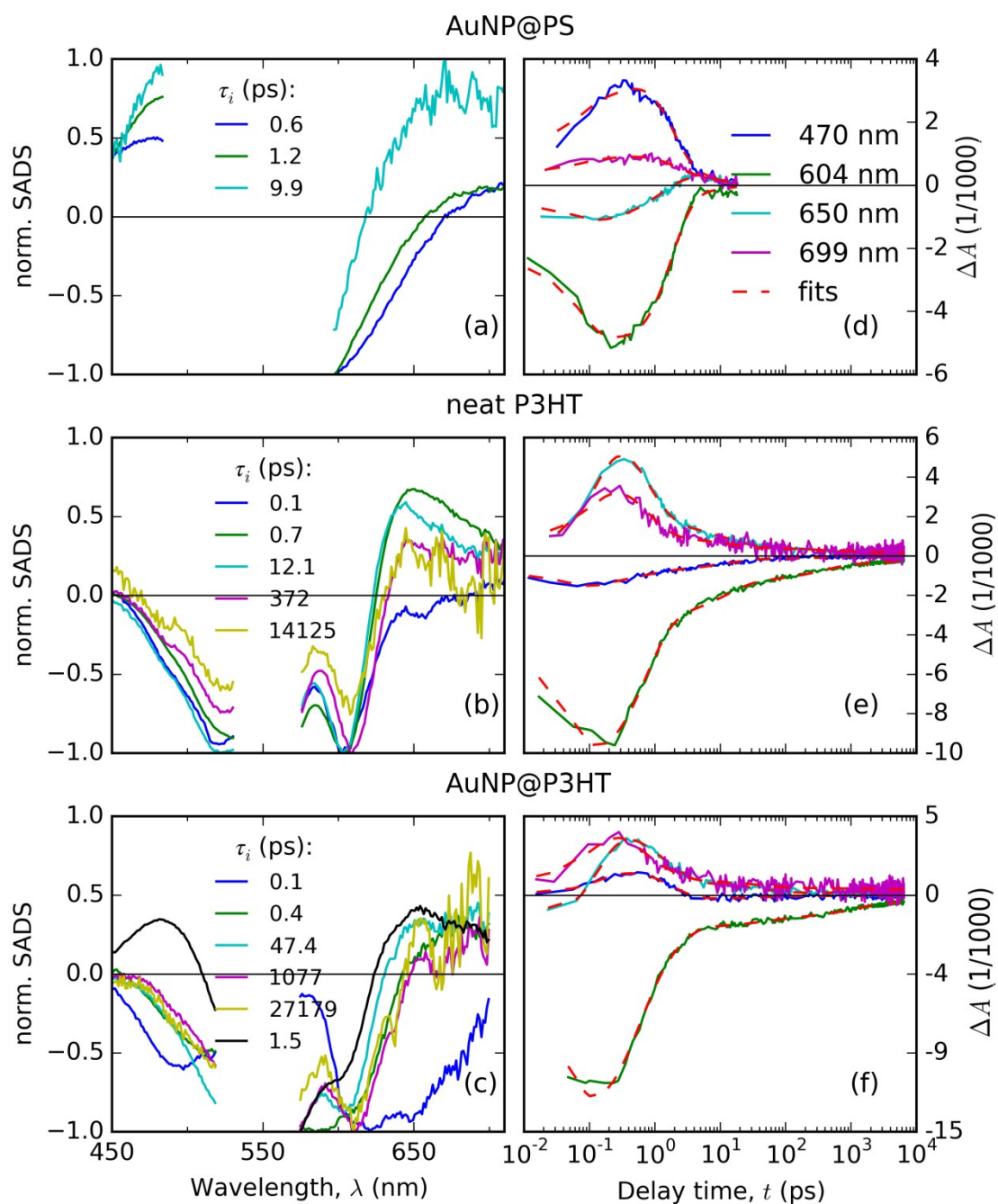


Figure S3. Comparison of the results of the *target analysis* of the TA data obtained on AuNP@PS (a,d), neat P3HT (b,e) and AuNP@P3HT composite films (c,f), using the model Eqs. (1 and 2). The respective Species-Associated Differential Spectra (SADS) were normalized to their respective peak value and are shown in the left column of panels (a–c), together with the respective decay time constants, τ_i , as indicated in the legends. Right panels

(d–f) show the experimental signal evolutions and the respective fitted curves at selected probe wavelengths.

Table S1. Summary of the lifetimes obtained from the measured TA data observed in neat P3HT as well as the AuNP@P3HT. Errors are specified as 95 % confidence intervals.

<i>i</i>	τ_i	
	neat P3HT	AuNP@P3HT
1	0.115 ± 0.005	0.106 ± 0.002
2	0.68 ± 0.02	0.42 ± 0.02
3	12.1 ± 0.4	47 ± 4
4	372 ± 20	1078 ± 80
5	14100 ± 1600	27000 ± 11000
6^{Au}		1.50 ± 0.05

^{Au} State attributed to the excited plasmon in AuNPs array.

Spectral analysis of the NIR-probe TA data

The spectral model function:

$$\Delta A^M(\lambda_{pr}, t) = \sum_{i=1}^2 J(\lambda_{pr}) H_i(t) \exp \left\{ -\frac{\left(\frac{hc}{\lambda_{pr}} - E_i^{center} \right)^2}{2\sigma_i^2} \right\}, \quad (3)$$

was a sum of two Gaussians in energy scale with time-invariant central photon energies E_i^{center} and half-widths, σ_i , and the time-dependent heights (amplitudes) $H_i(t)$. The Gaussians were transformed to the wavelength scale with the help of Jacobian factor $J(\lambda_{pr}) = hc/\lambda_{pr}^2$.

We have analyzed the FFT filtered datasets of the experimental NIR-probe TA data, $\Delta A(\lambda, t)$, by using the spectral model function by two-tier fitting algorithm (called here *master*). In the higher-tier, the time-invariant parameters E_i^{center} and σ_i were optimized by Levenberg–Marquardt algorithm (LMA)⁶ for the whole spectro-temporal dataset (globally), whereas in the lower-tier fitting we optimized $H_i(t)$ in Eq (3) by non-negative linear least-squares algorithm (NNLS)⁷ at each delay time t separately. In each iteration of the *master*, the LMA generated model function ΔA^M with trial parameters E_i^{center} and σ_i , which was then passed to

NNLS for the optimization of $H_i(t)$. The NNLS returned fit error value err to the LMA, as a feedback of the quality of the model time-invariant parameters:

$$err = \sum_t \sum_{\lambda_{pr}} \frac{(\Delta A(\lambda_{pr}, t) - \Delta A^M(\lambda_{pr}, t))^2}{(\Delta A(\lambda_{pr}, t) - \widehat{\Delta A}(\lambda_{pr}, t))^2}. \quad (4)$$

After the fit converged, the LMA generated the resulting best-fitting values for each time-invariant parameter, and estimated their standard errors, as summarized in Table S2.

The presented results of the fit were almost always optimal, as can be deduced from the representative fit results presented in Figures S4 and S5).

The resulting best-fit series of $H_i(t)$ were generated using the best-fit values of the time-invariant parameters with the unconstrained linear least-squares algorithm⁸ (LSQR) for each delay time t .

The reason for choosing the nonnegative version of least-squares algorithm (NNLS) for the optimization of the time-invariant parameters is that only the positive amplitudes $H_i(t)$ are physically meaningful. Using the unconstrained LSQR was necessary to remove the bias induced by NNLS, due to the fact that it yielded $H_i(t)=0$ in the cases where the unconstrained related algorithm, the LSQR, would use negative value. This was obvious mostly in the longer delay time range, where the noise in the data was greater than the mean value of the TA signal.

The $H_1(t)$ has been assigned in the main text to the concertation of singlet excitons, $C_S(t)$, and $H_2(t)$ has been assigned to free polarons $C_{FP}(t)$.

Table S2. Parameters of Gaussian spectral model found with the spectral analysis. Numerical values are in (eV) units. Parameters with lower index 1 and 2 are interpreted as exciton and polaron TA signals, respectively.

parameter	initial guess	neat P3HT		AuNP@P3HT	
		best fit	std. err.	best fit	std. err.
E_1^{center}	1.0	0.96	0.14	0.96	0.14
σ_1	0.3	0.19	0.15	0.18	0.16
E_2^{center}	1.3	1.30	0.034	1.31	0.044
σ_2	0.1	0.16	0.05	0.15	0.05

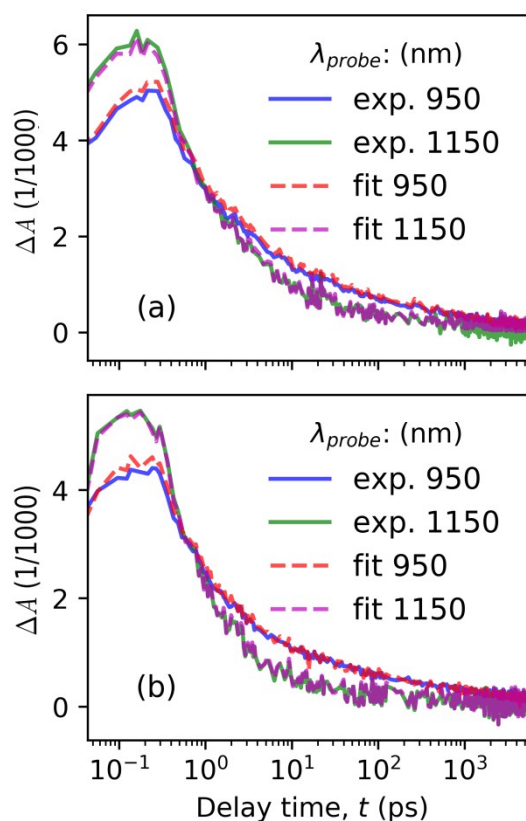


Figure S4. Estimation of fitting quality. Comparison of selected time traces of filtered experimental data and the respective fitted curves of (a) neat P3HT and (b) AuNP@P3HT samples. Probe wavelengths are indicated in legends.

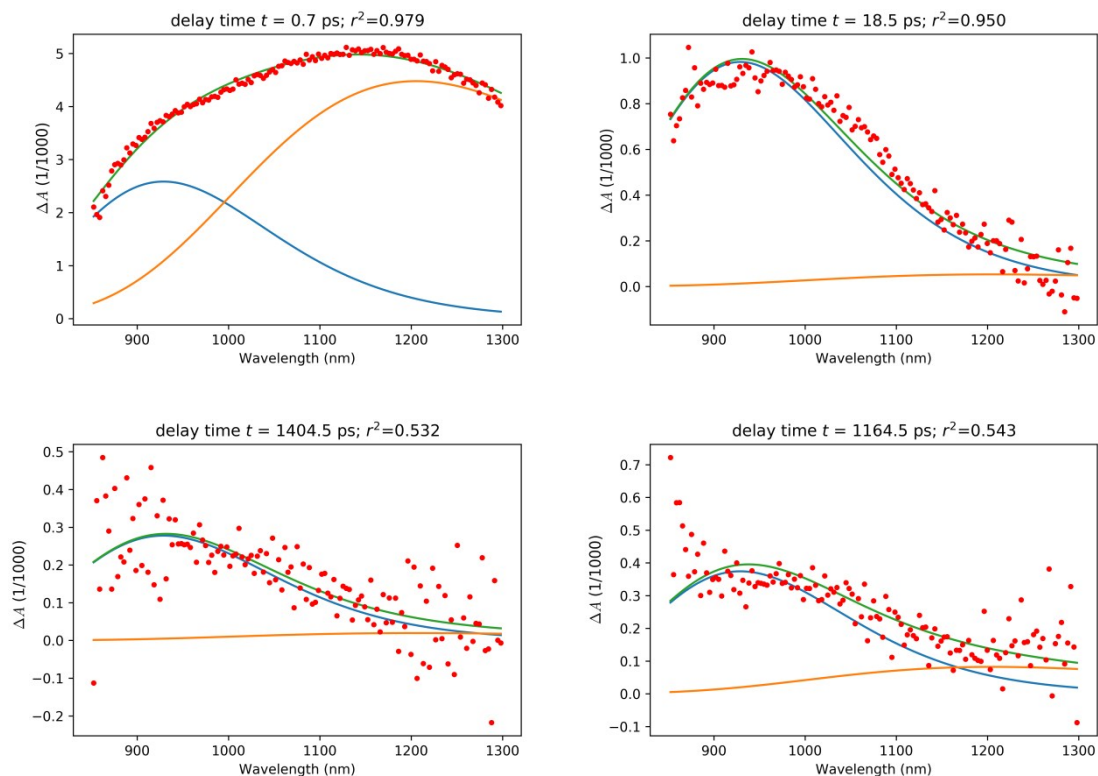


Figure S5. A representative example of fit results of the spectral model for the neat P3HT film at the respective delay times (as indicated above each plot together with r^2 coefficient of determination). In the top row of graphs, these there are the fits with the two highest r^2 values; in the lower row examples of those fits with values of r^2 about 0.539 (the median value.) are shown

Thermochromic effect in TA experiment

We calculated the thermochromic effect ΔA_{thermo} from the temperature, T , dependent steady-state absorbance spectra $A(T)$ published in ref. ⁹ as: $\Delta A_{\text{thermo}} = A(130^\circ\text{C}) - A(110^\circ\text{C})$. In Figure S6, we show that it indeed overlaps quite well with the residual TA signal $\Delta A_{\text{AuNP@P3HT}} - \Delta A_{\text{P3HT}}$ averaged over delay time interval 1–2 ns presented in Figure 3c in the main text. Note that the residual TA signal was multiplied by factor 15 for better comparison.

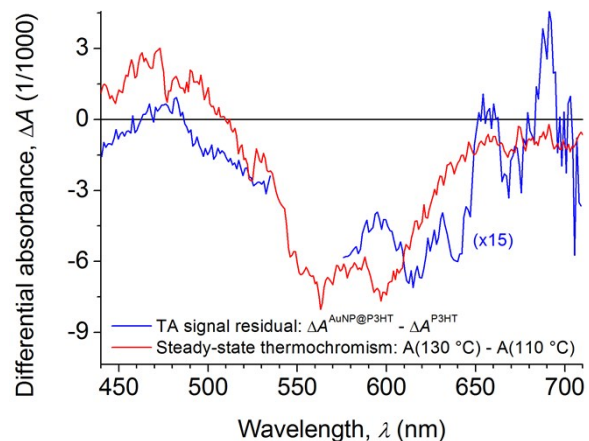


Figure S6. The thermochromic effect from the steady-state absorbance spectra published in ref.⁹ compared with the residual TA signal $\Delta A^{\text{AuNP@P3HT}}(t,\lambda) - \Delta A^{\text{P3HT}}(t,\lambda)$ averaged over the delay time interval of 1–2 ns. Note that the residual TA signal was multiplied by factor 15 for better comparison, and that the steady state spectra were measured at temperatures 130 °C and 110 °C.

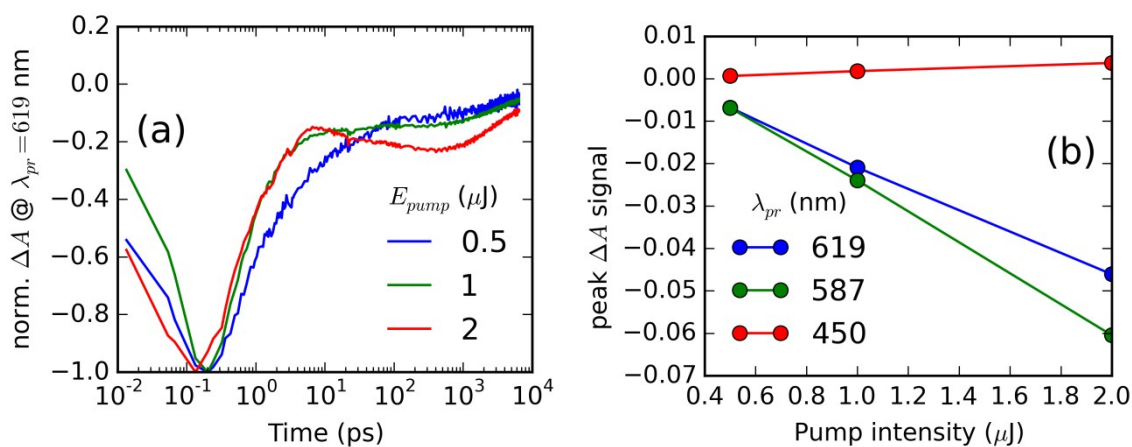


Figure S7. (a) The dependence of TA kinetics of the AuNP@P3HT sample on the total energy in the pump pulse energy (shown in the legend). With increasing energy, E_{pump} , from 0.5 to 1.0 μJ , the initial decay rate increased. Further E_{pump} increase affected mainly the later delay times. (b) The dependences of TA signal at selected probe wavelengths λ_{pr} (see the legend); all show linear characteristics.

REFERENCES

- (1) I. H. van Stokkum, D. S. Larsen and R. van Grondelle, *Biochim. Biophys. Acta, Bioenerg.*, 2004, **1657**, 82 – 104.
- (2) M. Ameloot, J. M. Beechem and L. Brand, *Chem. Phys. Lett.*, 1986, **129**, 211–219.
- (3) J. J. Snellenburg, S. P. Liptonok, R. Seger, K. M. Mullen and I. H. van Stokkum, *J. Stat. Soft.*, 2012, **49**, 1–22.
- (4) K. M. Mullen and I. H. van Stokkum, *J. Stat. Soft.*, 2007, **18**, 1–46.
- (5) J. M. Beechem, M. Ameloot and L. Brand, *Chem. Phys. Lett.*, 1985, **120**, 466 – 472.
- (6) `scipy.optimize.leastsq`, *SciPy v0.13.0 Reference Guide*, <https://docs.scipy.org/doc/scipy/reference/generated/scipy.optimize.leastsq.htm>, Retrieved 15 March 2017.
- (7) `scipy.optimize.nnls`, *SciPy v0.13.0 Reference Guide*, <http://docs.scipy.org/doc/scipy/reference/generated/scipy.optimize.nnls.html>, Retrieved 15 March 2017.
- (8) `numpy.linalg.lstsq`, *NumPy v1.12 Manual*, <https://docs.scipy.org/doc/numpy/reference/generated/numpy.linalg.lstsq.html>, Retrieved 15 March 2017.
- (9) B. Paruzel, E. Pavlova, J. Pflieger, M. Šlouf, K. Halašová and r. Mikmeková, *Chem. Pap.*, 2017, **71**, 401–408.